UCSF
UC San Francisco Previously Published Works

Title

Cooperative Blockade of PKCα and JAK2 Drives Apoptosis in Glioblastoma

Permalink

https://escholarship.org/uc/item/2c52w42q

Journal

Cancer Research, 80(4)

ISSN

0008-5472

Authors

Wong, Robyn A
Luo, Xujun
Lu, Mimi
et al.

Publication Date

2020-02-15

DOI

10.1158/0008-5472.can-18-2808

Peer reviewed

Cooperative blockade of PKCα and JAK2 drives apoptosis in glioblastoma

Robyn A. Wong[1,2,*], **Xujun Luo**[1,2,3,*], **Mimi Lu**[1,2], **Zhenyi An**[1,2], **Daphne A. Haas-Kogan**[4], **Joanna J. Phillips**[2,7], **Kevan M. Shokat**[5], **William A. Weiss**[1,2,6,7,#], **Qi Wen Fan**[1,2,#]

[1]Department of Neurology, University of California, San Francisco, CA 94158, USA

[2]Helen Diller Family Comprehensive Cancer Center, San Francisco, CA 94158, USA

[3]the Second Xiangya Hospital, Central South University, Changsha, Hunan 410011, China

[4]Department of Radiation Oncology, Harvard Medical School and Brigham and Women's Hospital, Dana-Farber Cancer Institute, Boston Children's Hospital, Boston, MA 02215, USA

[5]Howard Hughes Medical Institute and Department of Cellular and Molecular Pharmacology, University of California, San Francisco, CA 94158, USA

[6]Department of Pediatrics, University of California, San Francisco, CA 94158, USA

[7]Department of Neurological Surgery, University of California, San Francisco, CA 94158, USA

Abstract

The mechanistic target of rapamycin (mTOR) signaling is dysregulated prominently in human cancers including glioblastoma, suggesting mTOR as a robust target for therapy. Inhibitors of mTOR have had limited success clinically however, in part because their mechanism of action is cytostatic rather than cytotoxic. Here, we tested three distinct mTOR kinase inhibitors (TORKis) PP242, KU-0063794, and sapanisertib against glioblastoma cells. All agents similarly decreased proliferation of glioblastoma cells, whereas PP242 uniquely induced apoptosis. Apoptosis induced by PP242 resulted from off-target cooperative inhibition of Janus kinase 2 (JAK2) and protein kinase C alpha (PKCα). Induction of apoptosis was also decreased by additional on-target inhibition of mTOR, due to induction of autophagy. As EGFR inhibitors can block PKCα, EGFR inhibitors erlotinib and osimertinib were tested separately in combination with the JAK2 inhibitor AZD1480. Combination therapy induced apoptosis of glioblastoma tumors in both flank and in patient-derived orthotopic xenograft models, providing a preclinical rationale to test analogous combinations in patients.

Keywords

mTOR mechanistic target of rapamycin; TORKi; mTOR kinase inhibitor; JAK2; janus kinase 2; PKCα; protein kinase C alpha; GBM; glioblastoma

[#]Correspondence should be addressed to: Qi Wen Fan, Department of Neurology, University of California, San Francisco, 1450 3rd Street, San Francisco, CA94158-9001, Tel: (415) 502-1695, qiwen.fan@ucsf.edu; William A. Weiss, Department of Neurology, University of California, San Francisco, 1450 3rd Street, San Francisco, CA94158-9001, Tel: (415) 502-1694, waweiss@gmail.com.
[*]Equal Contribution: Robyn A. Wong, Xujun Luo

Introduction

Glioblastoma is the most common primary brain tumor. There is a profound disconnect between the ascertainment of impactful underlying biology, and the ability to translate that biology to improved outcomes for patients. A major need in glioblastoma is the identification of targeted agents that penetrate the brain, and that drive cytotoxicity.

Signaling from receptor tyrosine kinases (RTKs) to phosphatidylinositol 3' kinase (PI3K), AKT, and the mechanistic target of rapamycin (mTOR) occurs commonly in glioblastoma (1). Signaling between PI3K and mTOR is also frequently activated in the absence of upstream activation of RTKs, due to mutation or silencing of Phosphatase and TENsin homologue *(PTEN),* a negative regulator of PI3K. Activation of PI3K leads to phosphorylation and activation of AKT, a serine-threonine kinase and key negative regulator of apoptotic signaling (2).

A number of mTOR inhibitors are currently in clinical trials or advanced preclinical testing. Allosteric mTOR inhibitors including rapamycin and its analogs are selective for the mTORC1 target pS6 (3). Active site orthosteric mTOR kinase inhibitors (TORKis) including PP242, KU-0063794, sapanisertib (previously TAK-228/MLN0128/INK128) block ATP binding to mTOR kinase, resulting in inhibition of mTORC1 targets S6 kinase and 4EBP1, and mTORC2 targets including AKT (4–6).

Therapies targeting RTKs, P13K and mTOR are largely cytostatic in glioblastoma, resulting in a reservoir of cells poised to drive resistance and tumor progression. Here we confirm that inhibition of mTOR kinase also results in cytostasis in glioblastoma. Surprisingly however, the tool TORKi PP242 induced apoptosis in glioblastoma cells, in a manner independent of *PTEN* status. We demonstrate that apoptosis driven by PP242 resulted from off-target blockade of PKCα and JAK2. To translate these observations, we used an EGFR inhibitor to block PKCα, and combined this agent with a JAK2 inhibitor. Combination therapy drove cytotoxicity in vitro and in vivo, providing a combination approach potentially translatable to patients.

Materials and Methods

Cell lines, reagents, transfection, and transduction

Cell lines LN229 and U251 obtained from the Brain Tumor Research Center at UCSF were grown in DMEM with 10% FBS. Patient-derived xenograft (PDX) glioma specimens GBM6, GBM8. GBM12, GBM34, and GBM43 (7, 8) were obtained from Dr. C David James, were grown in neurobasal complete medium supplemented with 20 ng/ml EGF and 20 ng/ml FGF. All cell lines were authenticated from original source using short tandem repeat (STR) profiling and certified to be mycoplasma-free. LN229 and U251 cells were passaged less than 15 times after thawing. PDX-derived cell lines were passaged less than 5 times. In addition, mycoplasma status was monitored monthly in the lab using HEK-blue detection kit (InvivoGen, hb-det). Erlotinib tablets (Genentech) were pulverized and dissolved in HCL, and the aqueous phase was extracted with ethyl acetate. Combined

organic extracts were dried over sodium sulfate and concentrated. Inhibitors KU-0063794 (S1226), sapanisertib (S2811), gö6983 (S2911), AZD1480 (S2162), and osimertinib (S7297) were from Selleck Chemicals. EGF (REF 11376454001) was from Roche. TPA (4174S) and OSM (5367SC) were from Cell Signaling. JAK2 siRNA (L-003146–00-0005) and siRNA control were purchased from Dharmacon. Cells were transfected with siRNA using Lipofectamine 2000 (Invitrogen, 11668019) as directed by the manufacturer. PKCα shRNA (TRCN0000001693), and shRNA control were purchased from Sigma. Lentivirus was used to infect cells and selected for two weeks with puromycin (1.5 μg/ml). A constitutively active form of PKCα (PKCα-Cat), a gift from J-W Soh, was generated by deleting the regulatory N-terminal domain of PKCα (9). pHACE-PKCα-Cat plasmid was digested with EcoRI and ligated into a similarly pBabe-puro plasmid, generating retroviral-based pBabe-puro-PKCα-Cat. To generate retrovirus to transduce PKCα-Cat or EGFR, the packaging cell line 293T was co-transfected pBabe-puro-PKCα-Cat or pWLZ-hygro-EGFR plasmid, along with gag/pol, and VSVg using Effectene (Qiagen, 301425). High-titer virus collected at 48 hours was used to transduce cells as described (10). Transduced cells were selected as pools with puromycin (1.5 μg/ml) or hygromycin (500 μg/ml) for two weeks. JAK2 (V617F)-pcw107-V5 was a gift from David Sabatini & Kris Wood and was stably transfected into LN229:EGFR cells with Effectene. Transfected cells were selected as pools with puromycin (1.5 mg/ml) for 2 weeks.

Cell proliferation assays and apoptosis detection

For proliferation, 5×10^4 cells were seeded in 12-well plates and treated as indicated for three days. Proliferation was determined by WST-1 assay (Roche, 11644807001) and analyzed by spectrophotometry. Each sample was assayed in triplicate and absorbance at 450 nm read on a plate reader after 40 minutes. Background absorbance was subtracted from each condition, and then normalized to the untreated control. Apoptosis was detected by flow cytometry for annexin V-FITC per the manufacture's protocol (annexin V-FITC detection kit, BD Pharmingen, 556547), by western blotting for cleaved PARP, or by staining for cleaved caspase 3. Flow cytometry data was collected on a FACSCalibur (Becton Dickinson) using CellQuest software, then analyzed using FlowJo (v9) software.

Detection and quantification of AVOs

Cells were treated with indicated inhibitors for 48 hours, stained with acridine orange (1 μg/ml) for 15 minutes, washed with phosphate-buffered saline (PBS), trypsinized, and then collected in phenol red-free growth medium. Green (510 to 530 nm) and red (650 nm) fluorescence emissions from 1×10^5 cells illuminated with blue (488 nm) excitation light were measured with FACSCalibur from Becton-Dickinson with CellQuest software.

Western blotting

Membranes were blotted with p-EGFR^{Y1173} (Invitrogen, 44–794G), EGFR (SC-03), ERK2 (SC-154), p-PKCα^{S657} (SC-12356) (Santa Cruz Biotechnology), p-AKT^{S473} (9271S), AKT (4691S), p-ERK$^{T202/Y204}$ (4370S), p-RPS6$^{S235/236}$ (4858S), RPS6 (2217S), p-4EBP1$^{T37/46}$ (2855S), 4EBP1 (9644S), p-PKC (pan) (βII Ser660) (9371S), PKCα (59754S), p-MARCKS$^{S152/156}$ (2741S), MARCKS (5607S), p-STAT3^{Y705} (9145S), STAT3 (4904S), PARP (9532S), and JAK2 (3230S) (Cell Signaling), 4G10 (05–321), and GAPDH (AB2302)

(EMD Millipore). Bound antibodies were detected with HRP-linked anti-mouse (DC-02L) or anti-rabbit IgG (DC-03L) (Calbiochem), followed by ECL (Amersham, RPN2106).

JAK2 mRNA expression in human Glioblastoma, LGG, and normal brain

Expression mRNA levels of JAK2 from 163 patients with glioblastoma, 518 patients with low grade glioma, and 207 normal brain tissue samples were downloaded from GEPIA (dataset: TCGA-GBM, TCGA-LGG, GTEx). Comparison of expression data was performed using the online tool at http://gepia.cancer-pku.cn.

Xenografts

GBM34 cells (5×10^6) were injected subcutaneously in the right flank of four to six weeks old female athymic BALB/C$^{nu/nu}$ nude mice (Simonsen Laboratories). After tumors were established (50 to 100 mm^3), seven mice per group were randomly allocated to treatment with vehicle (0.5% HPMC, 0.1% Tween 80 in H_2O), 50 mg/kg erlotinib, 15 mg/kg AZD1480, or 50 mg/kg erlotinib plus 15 mg/kg AZD1480, delivered by daily oral gavage for 15 days. Tumor diameters were measured daily with calipers, and tumor volumes (in cubic millimeters) were calculated: volume = width$^2 \times$ Length/2. Orthotopic injections and treatment studies: Female BALB/C$^{nu/nu}$, mice (four to six weeks old) were anesthetized with isoflurane inhalation. GBM43 cells (7×10^4) expressing firefly luciferase were injected intracranially (Hamilton syringe) at coordinates 2 mm anterior and 1.5 mm lateral of the right hemisphere relative to Bregma, at a depth of 2.5 mm. Whole brain bioluminescence was measured for each mouse every three to four days. When bioluminescence reached 10^6 photons per second, mice were sorted into four groups of equal mean bioluminescent signal (6 mice per group), and therapy initiated. Mice were treated with vehicle (0.5% HPMC, 0.1% Tween 80 in H_2O), 25 mg/kg osimertinib, 30 mg/kg AZD1480, or 25 mg/kg osimertinib plus 30 mg/kg AZD1480, delivered by daily oral gavage for 15 days. Mice were monitored daily and euthanized when they exhibited neurological deficits or 15% reduction from initial body weight.

Histological and immunohistochemical analyses

For indirect immunofluorescence, GBM34 tumor tissue was removed and fixed in 4% paraformaldehyde in PBS at 4°C for 4 hours, followed by overnight incubation in 20% sucrose (in PBS) at 4°C. Specimens were embedded in OCT compound. Sections of 10 μm thickness were cut, placed on silane-coated glass, and subjected to cleaved caspase3 and nuclear staining as described previously (11). GBM43 tumor tissue, brain, heart, lung, kidney, and liver were removed and fixed in 4% paraformaldehyde in PBS at 4°C for 24 hours, tissues were then paraffin-embedded, and sectioned (10 μm) for hematoxylin and eosin (H&E) staining, histopathological, and immunohistochemical analyses. For immunohistochemistry (IHC), slides were deparaffinized, and antigen retrieval was performed using a pressure cooker. The VECTASTAIN ABC reagent (Vector laboratories, PK-4000) was used for signal detection. The Cleaved-Caspase 3 (Cell Signaling, 9661L) and Ki67 (Cell Signaling, 9027S) antibodies were used at a concentration of 1:100. Images were taken using a Nikon Eclipse microscope.

Animal study approval

Animal experiments were conducted using protocols approved by University of California, San Francisco's Institutional Animal Care and Use Committee (IACUC).

Statistical analysis

For survival analysis, log-rank test was used. For other analyses, a two-tailed paired Student's t-test was applied.

Results

TORKi PP242 induces apoptosis in glioblastoma

We compared three distinct TORKis: KU-0063794, PP242, and sapanisertib for impact on proliferation and apoptosis. All glioma cell lines tested showed dose-dependent decreases in cell proliferation detected by WST-1 assay. This effect was independent of *PTEN* and *EGFR* status (Fig. 1A; Supplementary Fig. S1A). Flow cytometric analysis using the apoptotic marker annexin V, and immunoblotting for the apoptotic marker cleaved PARP demonstrated apoptosis uniquely in response to PP242 (Fig. 1B and C; Supplementary Fig. S1B and C). As expected, all three mTOR kinase inhibitors blocked phosphorylation of AKT, RPS6, and 4EBP1 in dose-dependent fashion (Fig. 1C; Supplementary Fig. S1C). Interestingly, GBM6 cells expressing the constitutively active tumor-derived EGFRvIII allele were resistant to apoptosis induced by PP242, with no impact on mTOR signaling and cell proliferation in response to PP242 (Supplementary Fig. S1A–C).

Apoptosis can be induced through release of internal or external stimuli (intrinsic or extrinsic pathways) (12). To clarify whether the BAX-dependent intrinsic pathway was activated in response to PP242, we examined the ability of PP242 to induce apoptosis in *BAX* wild -type and *BAX*-deficient mouse embryonic fibroblasts (13). Treatment with PP242 led to apoptosis only in cells wild-type for BAX as measured by annexin V flow cytometry and by PARP cleavage. (Supplementary Fig. S1D and E), demonstrating mitochondrial dependence.

PP242 inhibits mTOR, PKCα, and JAK2

PP242 was unique among TORKis in inducing apoptosis, suggesting an off-target effect. Among 219 kinases previously assayed, only four: mTOR, PKCα, p110γ, and JAK2 were inhibited significantly by PP242 in vitro (IC_{50} values 8, 49, 102, and 110 nM, respectively) (4). We have shown previously that inhibitors of PI3K p110γ had no effect on proliferation or apoptosis of glioma cells (11). It is therefore unlikely that inhibition of p110γ contributed to the apoptotic effect of PP242 (Fig. 2A). To verify that PP242 could inhibit these targets in glioma cells, we evaluated PKCα and JAK2 blockade, comparing PP242, KU-0063794, and sapanisertib. PP242 uniquely inhibited the PKC substrate p-MARCKS$^{S152/156}$ and the JAK2 target p-STAT3^{Y705} in a dose dependent manner, validating PKC and JAK2 as targets of PP242. PP242 showed a dose-dependent blockade of p-STAT3^{Y705} in all lines and short-term PDX cultures, although less prominently in PDX GBM6. (Fig. 2B and C; Supplementary Fig. S2A and B). Among six lines and short term PDX cultures tested, GBM6 was also resistant to apoptosis induced by PP242 (Supplementary Fig. S1B and C).

Inhibition of PKCα and JAK2 but not mTOR drives apoptosis

To separately probe roles for PKCα, JAK2, and mTOR in PP242-driven apoptosis, we analyzed the PKC inhibitor gö6983 (14), the JAK2 inhibitor AZD1480 (15), and the apoptosis-sparing TORKi sapanisertib (6). We assessed proliferation, apoptosis, and phosphorylation of PKCα, STAT3, RPS6, and 4EBP1 following treatment of LN229 and U251 glioblastoma cells. The PKC inhibitor gö6983 reduced levels of both p-PKCα^{S657} and total PKC in a dose dependent manner. Apoptosis was increased at high doses, with little effect on proliferation in LN229 cells and modestly blocking proliferation in U251 cells (Fig. 3A–C, **left panel;** Supplementary Fig. S3A–C, left panel). The JAK2 inhibitor AZD1480 decreased levels of p-STAT3^{Y705} in a dose dependent manner, modestly blocking proliferation and inducing apoptosis at high doses in both cell lines (Fig. 3A–C, **middle panel;** Supplementary Fig. S3A–C, middle panel). Consistent with a central role for mTOR in the regulation of cell growth, the TORKi sapanisertib showed a dose-dependent reduction in proliferation, associated with decreased levels of p-RPS6$^{S235/236}$ and p-4EBP1$^{T37/46}$; without appreciably inducing apoptosis (Fig. 3A–C, **right panel;** Supplementary Fig. S3A–C, right panel).

Inhibition of PKCα, JAK2, and autophagosome maturation induces maximal apoptosis

We next assessed combination therapy. Blockade of PKC and JAK2 cooperated to induce apoptosis, measured by annexin V flow cytometry, and PARP cleavage. Combining inhibitors of PKC and mTOR kinase, or JAK2 with mTOR kinase did not induce apoptosis in any of three human glioblastoma cell lines (Fig. 4A and B; Supplementary Fig. S4A and B). As expected, further inhibition of p110 γ using p110γ inhibitor AS-252424 did not induce additional apoptosis in the setting of blockade of PKC and JAK2 (Supplementary Fig. S4C). To address relevance, we analyzed mRNA expression of JAK2 in human normal brain, glioblastoma and low grade glioma (LGG) from GTEx and TCGA databases. Levels of JAK2 mRNA were significantly lower in normal brain, compared to glioblastoma and low-grade glioma (Supplementary Fig. S4D).

The JAK2 inhibitor AZD1480 potently blocked p-STAT3^{Y705}, with little impact on p-STAT5^{T694}, suggesting that apoptosis was induced using AZD1480 in combination with gö6983 might be more dependent on the JAK2/STAT3 rather than the JAK2/STAT5 signaling pathway (Supplementary Fig. S4E). We validated JAK2 and PKCα dependence using RNAi. Since PKCα has a long half-life (16), stable cell lines expressing shRNA against PKCα were generated in LN229 and U251 parent cell lines (Fig. 4C; Supplementary Fig. S4F and G). Combining PKCα shRNA with the JAK2 inhibitor AZD1480 or combining JAK2 siRNA with PKC inhibitor Gö6983 also enhanced apoptosis in LN229 and U251 cells (Supplementary Fig. S4F and G). Consistent with our results using small molecule inhibitors in combination, and combining small molecule inhibitors with RNAi against JAK2 and/or PKCα, RNAi against JAK2 and PKCα in combination could also drive apoptosis. (Fig. 4A–C; Supplementary Fig. S4A and B and S4F and G).

Interestingly, apoptosis was markedly decreased in triple combination (PKCα, JAK2, and mTOR inhibitors) as compared to double combination with PKC and JAK2 inhibitors (Fig. 4A and B; Supplementary Fig. S4A and B). We have previously shown that the TORKi

KU-0063794 induced autophagy that could partially block apoptosis in glioblastoma (10). We therefore asked whether PP242 could also induce autophagy, and whether autophagy induced in response to mTOR kinase inhibition represented a survival pathway that abrogated apoptosis induced by blockade of JAK2 and PKCα. We measured induction of autophagy by staining for acridine orange, which moves freely across biological membrane and accumulates in acidic vesicle organelles (AVOs) associated with autophagy; and by western blotting for the conversion of LC3-I to LC3-II, a marker of autophagy. As expected, PP242 induced appreciable AVOs. and LC3-II conversion (Fig. 4D; Supplementary Fig. S4H). Having confirmed that PP242 was able to induce autophagosome formation, we next asked whether PP242 could drive apoptosis in cooperation with bafilomycin A1 (Baf A1), which inhibits the vacuolar-type H^+-ATPase and thereby blocks autophagosome maturation (17). Baf A1 treated cells showed increased conversion of LC3–1 to LC3-II, due to autophagosome accumulation, and had little effect on apoptosis. Combining PP242 with Baf A1 induced maximal apoptosis, measured by annexin V flow cytometry (Student's t test, p = 0.0046, DMSO versus PP242 plus Baf A1; p = 0.0324, PP242 versus PP242 plus Baf A1; p = 0.0054, Baf A1 versus PP242 plus Baf A1) (Fig. 4D, **top panel**) and cleavage of PARP by western blotting (Fig. 4D, **bottom panel**).

To address the importance of PKCα and JAK2 inhibition to induction of apoptosis driven by PP242, we next determined whether activation of PKCα or JAK2 could rescue the apoptotic effect of PP242. LN229 cells were transduced with a dominant-active construct, PKCα-Cat (9) or transfected with a gain-of-function $JAK2^{V617F}$ mutant allele (18). The abundance of PKCα-Cat protein was less than that of endogenous PKCα (Fig. 4E) and the introduction of $JAK2^{V617F}$ led to increased phosphorylation of STAT3^{Y705} (Fig. 4F). The apoptotic effect of PP242 was partially abrogated either by PKCα-Cat or $JAK2^{V617F}$, measured by annexin V flow cytometry {Student's t test, p = 0.0044, PP242 (vector) versus PP242 (PKCα-cat), Fig. 4E, **top panel**; p = 0.0014, PP242 (vector) versus PP242 ($JAK2^{V617F}$), Fig. 4F, **top panel**} and by cleavage of PARP (Fig. 4E and F, **bottom panels**). Data in Fig. 4 indicated that inhibition of PKCα and JAK2 as off-targets of PP242 drive apoptosis. Additional blockade of mTOR kinase by PP242 partially rescues apoptosis, in-part through the induction of autophagy in glioblastoma cells.

Inhibitors of EGFR and JAK2 cooperate to induce apoptosis, in-part through inhibition of PKCα

PP242 is a tool compound with metabolic liabilities that preclude clinical development. The PKC inhibitor gö6983 is also a tool compound that has not been advanced clinically. Although AZD1480 has recently been withdrawn from development, it serves as a valuable probe compound to evaluate the role of JAK/STAT signaling in tumor models. Since the EGFR inhibitor erlotinib can block PKCα in glioma cells (16), we asked whether erlotinib would cooperate with the JAK2 inhibitor AZD1480 to induce apoptosis in patient derived xenograft (PDX) models. Prior to evaluating efficacy in vivo, we assessed the impact of combining erlotinib and AZD1480 in patient-derived GBM34 and in LN229:*EGFR* cells. Combined treatment with erlotinib and AZD1480 induced a 3.6 to 4.7-fold increase in apoptosis (annexin V-FITC positive cells) compared with DMSO control. Induction of apoptosis was associated with decreased abundance of phosphorylated signal transducer and

activator of transcription 3 protein (p-STAT3^{Y705}). As expected, EGF treatment induced phosphorylation of PKC, MARCKS, and STAT3, abrogated in response to erlotinib, while JAK2 inhibitor AZD1480 decreased phosphorylation of STAT3, with no impact on phosphorylation of PKC (Fig. 5A and B; Supplementary Fig. S5A and B). Similar results were obtained combining the third-generation EGFR Tyrosine kinase inhibitor (EGFR TKI) osimertinib with AZD1480 in GBM43 cells. Combined treatment with osimertinib and AZD1480 induced a 3.3 fold increase in apoptosis (annexin V-FITC positive cells) compared with DMSO control. Induction of apoptosis was again associated with decreased abundance of p-STAT3^{Y705} (Fig. 5C and D).

To address the importance of PKCα in apoptosis driven by EGFR inhibition in combination with JAK2 inhibitor, we next determined whether activation of PKCα could rescue the effect of the combination therapy on apoptosis, LN229:*EGFR* cells were transduced with a dominant-active construct, PKCα-Cat (9). The apoptotic effect of combination treatment was partially abrogated by PKCα-Cat, measured by annexin V flow cytometry {Student's *t* test, p = 0.0018, erlotinib plus AZD1480 (PKCα-Cat) versus erlotinib plus AZD1480 (vector)} and by cleavage of PARP (Fig. 5E and F). Data in Fig. 5 indicate that inhibitors of EGFR and JAK2 in combination drive apoptosis in glioblastoma cells, in-part through inhibition of PKCα.

Inhibitors of EGFR and JAK2 cooperate to induce apoptosis in patient-derived flank and orthotopic glioblastomas xenograft models

To translate these results to an in vivo setting, 5×10^6 GBM34 cells were implanted into nude mice subcutaneously (patient derived xenograft). Mice with established flank tumors were randomized into four groups (seven mice per group) and treated daily by oral gavage, with vehicle, erlotinib (50 mg/kg), AZD1480 (15 mg/kg), or erlotinib (50 mg/kg) plus AZD1480 (15 mg/kg). We assessed tumor burden, body weight, and apoptosis. Both erlotinib and AZD1480 showed single agent efficacy. Tumor sizes in mice treated with erlotinib and AZD1480 in combination were significantly smaller than either vehicle or monotherapy-treated controls (Student's *t* test, p = 0.0177, erlotinib plus AZD1480 versus vehicle; p = 0.0457, erlotinib plus AZD1480 versus erlotinib; p = 0.00373, AZD1480 plus erlotinib versus AZD1480) (Fig. 6A and B). Neither agent as monotherapy induced appreciable apoptosis. Erlotinib and AZD1480 led to combinatorial efficacy in driving apoptosis in vivo, with 10.6% of tumor cells staining positively for cleaved caspase 3, compared with 0.2% for tumors treated with vehicle, 1.6% for tumors treated with erlotinib, and 1.2% for tumors treated with AZD1480 as monotherapy (Fig. 6C). The treatment was well tolerated, with no loss of body weight (Supplementary Fig. S5C).

To extend these data, we next evaluated cooperative efficacy of EGFR and JAK2 inhibition in a patient-derived GBM43 orthotopic xenograft model. The third-generation EGFR inhibitor osimertinib has greater penetration of the blood-brain barrier (BBB) than the first-generation EGFR inhibitor erlotinib (19), and was therefore used for this study. Having confirmed that combined treatment with osimertinib and AZD1480 induced apoptosis in GBM43 in vitro (Fig. 5C and D), we next established intracranial xenografts (six mice per group), and treated mice daily by oral gavage with vehicle, osimertinib (25 mg/kg),

AZD1480 (30 mg/kg), or osimertinib (25 mg/kg) plus AZD1480 (30 mg/kg). We again assessed tumor burden, body weight, and apoptosis. Both osimertinib and AZD1480 showed single agent efficacy. Tumor sizes in mice treated with osimertinib and AZD1480 in combination were smaller than either vehicle or monotherapy-treated controls as assessed by luciferase signal (Fig. 6D; Supplementary Fig. S5D). Combination therapy was well tolerated, with no loss of body weight (Supplementary Fig. S5E). We followed mice on therapy for three weeks.

Combination therapy resulted in significantly improved survival (Student's t test, p = 0.0006, vehicle versus osimertinb plus AZD1480; p = 0.024, osimertinib versus osimertinib plus AZD1480; p = 0.0198, AZD1480 versus osimertinib plus AZD1480; log-rank analysis; n = 6 mice per group) (Fig. 6E). Osimertinib and AZD1480 led to combinatorial efficacy in driving apoptosis and decreased cell proliferation in orthotopic tumors in vivo, with 17.5% and 20% of tumor cells staining positively for cleaved caspase 3 and Ki67 respectively, compared with 1.8% and 56.6% for tumors treated with vehicle, 6.8% and 43.6% for tumors treated with osimertinib, and 4.1% and 35% for tumors treated with AZD1480 as monotherapy (Fig. 6F). We also evaluated toxicity. Histopathological examination showed no abnormalities in brain, heart, lung, and kidney from treated mice. Patchy areas of mild hepatic microvesicular steatosis were observed in the combination group. However, neither inflammation nor ballooning hepatocyte degeneration were seen (Supplementary Fig. S5F). Collectively, these data suggest that combined inhibition of PKC and JAK2 can drive apoptosis in glioblastoma in-vivo with minimal toxicity, offering a therapeutic rationale translatable to patients.

Discussion

Glioblastoma shows intrinsic resistance to most medical therapies. Currently, there are no curative treatment options for glioblastoma, despite decades of research. The signaling cascade linking RTKs, PI3K/AKT and mTOR is among the most frequently altered pathways in glioblastoma. While a number of small molecules target this axis, these predominantly result in cytostasis rather than cytotoxicity, leaving behind a reservoir of glioma cells that can drive relapse.

In screening three distinct mTOR kinase inhibitors (TORKi), we identified PP242 as unique among other TORKis in potently inducing apoptosis in glioma. We identified PKCα and JAK2 as off-targets critical to the ability of PP242 to induce apoptosis in glioma, and subsequently demonstrated that the TORKi component of PP242 actually blocked induction of apoptosis, inducing autophagy as a survival pathway. Among six lines and short-term PDX cultures tested, GBM6 was the most resistant to both blockade of STAT3 signaling, and to apoptosis induced by PP242. It may be pertinent in this regard, that GBM6 is reported to express high levels of EGFRvIII and low levels of wild-type EGFR (7, 8). Heterodimerization of EGFRvIII but not wild-type EGFR with the cytokine oncostatin M receptor (OSMR) has been shown to drive STAT3 signaling (20), potentially providing insights into the relative resistance of this line.

The PKC family of serine/threonine-specific protein kinases is organized into three groups according to activating domains (21). We and others have shown that PKCα is involved in survival and proliferation of glioma cells, suggested PKCα as a therapeutic target in GBM (16). JAK2 is a member of the Janus kinase family of non-receptor protein tyrosine kinases (22). JAK2 phosphorylates STAT3 (23). JAK2/STAT3 signaling is commonly dysregulated in GBM in part through activation by upstream receptor tyrosine kinases (RTKs) such as EGFR (24). JAK/STAT activation is correlated with higher grade gliomas and is a prognostic indicator of decreased survival (25). JAK2/STAT3 signaling plays important roles in tumor cell proliferation, survival, invasion and immunosuppression (26), suggesting JAK-STAT signaling as an attractive target for therapy in glioblastoma. STAT3 plays an important role in conferring resistance to therapy in glioblastoma (27). Do inhibitors of PKCα and JAK2 induce apoptosis through blockade of p-STAT3? Combined inhibition of PKCα and JAK2 decreased levels of p-STAT3^{Y705} more than observed using either agent as monotherapy, associated with a marked increase in apoptosis (Fig. 4B; Supplementary Fig. S4A and B).

We identified key targets required for apoptosis from a multi-targeted inhibitor, as a strategy to identify and evaluate effective combinations. This approach identified inhibition of PKCα and JAK2 as cooperating to drive apoptosis in glioblastoma. We demonstrated that inhibitors of EGFR could block PKCα, and that inhibitors of EGFR cooperated with inhibitors of JAK2 to induce apoptosis in flank and in patient-derived orthotopic xenograft models of glioblastoma in vivo, representing a translatable approach to drive cytotoxicity.

Supplementary Material

Refer to Web version on PubMed Central for supplementary material.

Acknowledgements

References

1. Brennan CW, Verhaak RGW, McKenna A, Campos B, Noushmeher H, Salama SR, et al. The somatic genomic landscape of glioblastoma. Cell 2013;155:462–77. [PubMed: 24120142]

2. Janku F, Yap TA, Meric-Bemstam F. Targeting the PI3K pathway in cancer: are we making headway? Nat Rev Clin Oncol 2018;5:273–91.

3. Saxton RA, Sabatini DM. mTOR signaling in growth, metabolism, and disease. Cell 2017;168:960–76. [PubMed: 28283069]

4. Feldman ME, Apsel B, Uotila A, Loewith R, Knight ZA, Ruggero D, et al. Active-site inhibitors of mTOR target rapamycin-resistant outputs of mTORC1 and mTORC2. Plos Biol 2009;7:e38. [PubMed: 19209957]

5. Garcia-Martinez JM, Moran J, Clarke RG, Gray A, Cosulich SC, Chresta CM, et al. Ku-0063794 is a specific inhibitor of the mammalian target of rapamycin (mTOR). Biochem J 2009;421:29–42. [PubMed: 19402821]

6. Hsieh AC, Liu Y, Edlind MP, Ingolia NT, Janes MR, Sher A, et al. The translational landscape of mTOR signaling steers cancer initiation and metastasis. Nature 2012;485:55–61. [PubMed: 22367541]

7. Sarkaria JN, Yang L, Grogan PT, Kitange GJ, Carlson BL, Schroeder MA, et al. Identification of molecular characteristics correlated with glioblastoma sensitivity to EGFR inhibition through use of an intracranial xenograft test panel. Mol Cancer Ther 2007;6:1167–74. [PubMed: 17363510]

8. Sarkaria JN, Carlson BL, Schroeder MA, Grogan P, Brown PD, Giannini C, et al. Use of orthotopic xenograft model for assessing the effect of epidermal growth factor receptor amplification on glioblastoma radiation response. Clin Cancer Res 2008;12:2264–71.15.

9. Soh JW, Lee EH, Prywes R, Weinstein IB. Novel roles of specific isoforms of protein kinase C in activation of the c-fos serum response element. Mol Cell Biol 1999;19:1313–24. [PubMed: 9891065]

10. Fan QW, Cheng C, Hackett C, Feldman M, Houseman BT, Nicolaides T, et al. Akt andAutophagy cooperate to promote survival of drug-resistant glioma. Sci Signal 2010;3:ra81. [PubMed: 21062993]

11. Fan QW, Knight ZA, Goldenberg DD, Yu W, Mostov KE, Stokat D, et al. A dual PI3 kinase/mTOR inhibitor reveals emergent efficacy in glioma. Cancer Cell 2006;9:341–49. [PubMed: 16697955]

12. Dillon CP, Green DR. Molecular cell biology of apoptosis and necroptosis in cancer. AdvExp Med Biol 2016;930:1–23.

13. Peña-Blanco A and García-Sáez AJ. Bax, Bak and beyond – mitochondrial performance In apoptosis. FEBS J 2018;3:416–31.

14. Gschwendt M, Dieterich S, Rennecke J, Kittstein W, Mueller HJ, Johannes FJ. Inhibition of protein kinase C mu by various inhibitors. Differentiation from protein kinase c isoenzymes. FEBS Lett 1996;392:77–80. [PubMed: 8772178]

15. Hedvat M, Huszar D, Hermann A, Gozgit JM, Schroeder A, Sheehy A, et al. The JAK2 inhibitor AZD1480 potently blocks Stat3 signaling and oncogenesis in solid tumors. Cancer Cell 2009;16:487–97. [PubMed: 19962667]

16. Fan QW, Cheng C, Knight ZA, Hass-Kogan D, Stokoe D, James CD, et al. EGFR signals to mTOR through PKC and independently of Akt in glioma. Sci Signal 2009;2:ra4. [PubMed: 19176518]

17. Yamamoto A, Tagawa Y, Yoshimori T, Moriyama Y, Masaki R, Tashiro Y, et al. Bafilomycin A1 prevents maturation of autophagic vacuoles by inhibiting fusion between Autophagosomes and lysosomes in rat hepatoma cell lines, H-4-II-E cells. Cell Struct Funct 1998;23:33–42. [PubMed: 9639028]

18. Kralovic R, Passamonti F, Buser AS, Teo SS, Tiedt R, Passweg JR, et al. A gain-of-function mutation of JAK2 in myeloproliferative disorders. N EngI J Med 2005;352:1779–90.

19. Ballard P, Yates JW, Yang Z, Kim DW, Yang JC, Cantarini M, et al. Preclinical comparison of osimertinib with other EGFR-TKIs in EGFR-mutant NSCLC brain metastasis models, and early evidence of clinical brain metastases activity. Clin Cancer Res 2016;22:5130–40. [PubMed: 27435396]

20. Jahani-Asl A, Yin H, Soleimani VD, Haque T, Luchman HA, Chang NC, et al. Control of glioblastoma tumorigenesis by feed-forward cytokine signaling. Nat Neurosci 2016;19:798–806. [PubMed: 27110918]

21. Isakov N Protein kinase C (PKC) isoforms in cancer, tumor promotion and tumor suppression. Semin Cancer Biol 2018;48:36–52. [PubMed: 28571764]

22. Hubbard SR. Mechanistic insights into regulation of JAK2 tyrosine kinase. Front Endocrinol (Lausanne) 2018;8:361. [PubMed: 29379470]

23. Stark GR, Darnell JE Jr. The JAK-STAT pathway at twenty. Immunity 2012;36:503–14. [PubMed: 22520844]

24. An Z, Aksoy O, Zheng T, Fan QW, Weiss WA. Epidermal growth factor receptor (EGFR) and EGFRvIII in glioblastoma (GBM): signaling pathway and targeted therapies. Oncogene 2018;37:1561–75. [PubMed: 29321659]

25. Bousoik E, Montazeri Aliabadi H. "Do We know jack" about JAK? a closer look at JAK/STAT signaling pathway. Front Oncol 2018;8:287. [PubMed: 30109213]

26. Atkinson GP, Nozell SE, Benveniste ET. NF-kappaB and STAT3 signaling in glioma: Targets for future therapies. Expert Rev Neurother 2010;10:575–86. [PubMed: 20367209]

27. Kim JE, patel M, Ruzevick J, Jackson CM, Lim M. STAT3 activation in glioblastoma: biochemical and therapeutic implications. Cancers (Basel) 2014;6:376–95. [PubMed: 24518612]
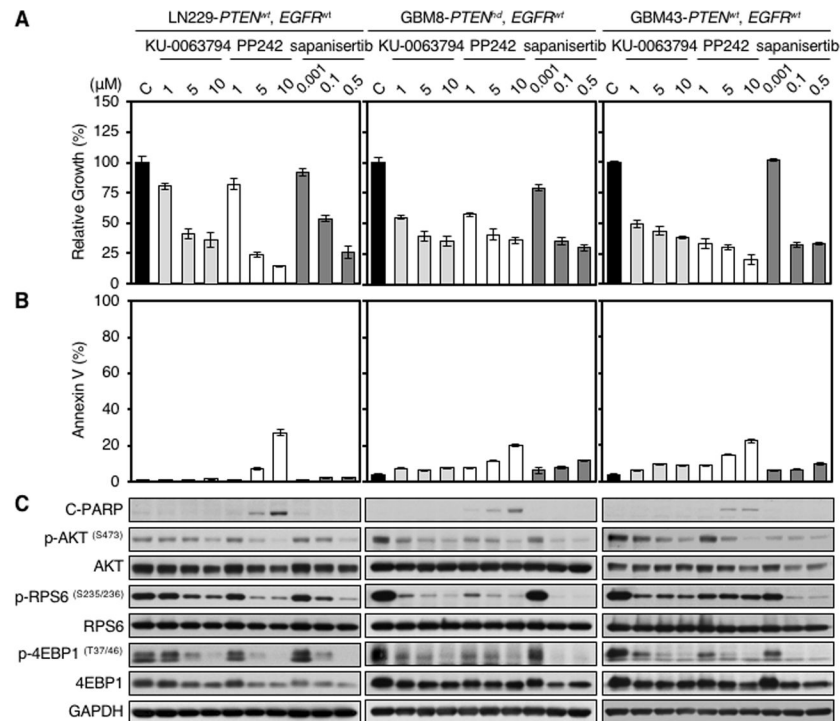
Significance

Findings identify PKCα and JAK2 as targets that drive apoptosis in glioblastoma, potentially representing a clinically translatable approach for glioblastoma.
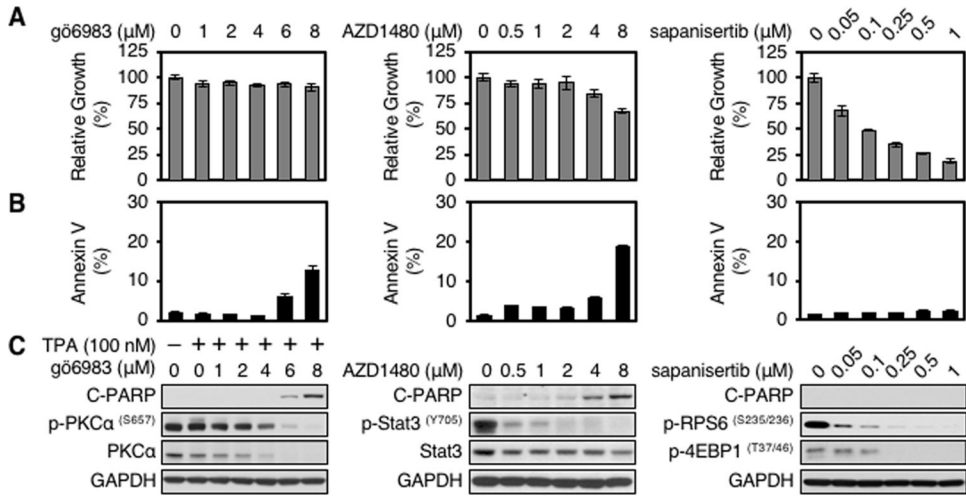
Figure 1.
TORKi PP242 induces apoptosis in glioma cells. LN229 parent, GBM8, and GBM43 cells were treated with KU-0063794, PP242, and sapanisertib at indicated doses for 72 hours. *PTEN and EGFR* status in glioma cell lines is shown (wt, wild type; hd, homozygous deleted). **A,** Proliferation was measured by WST-1 assay. Data shown represent mean ± SD (percentage of growth inhibition relative to DMSO-treated control) of triplicate measurements. **B,** Apoptosis was analyzed by flow cytometry for annexin V. Data shown represent mean ± SD (percentage of apoptotic cells relative to DMSO-treated control) of triplicate measurements. **C,** An aliquot of each lysate was analyzed by western blot with antibodies indicated. Blot representative of two independent experiments is shown.
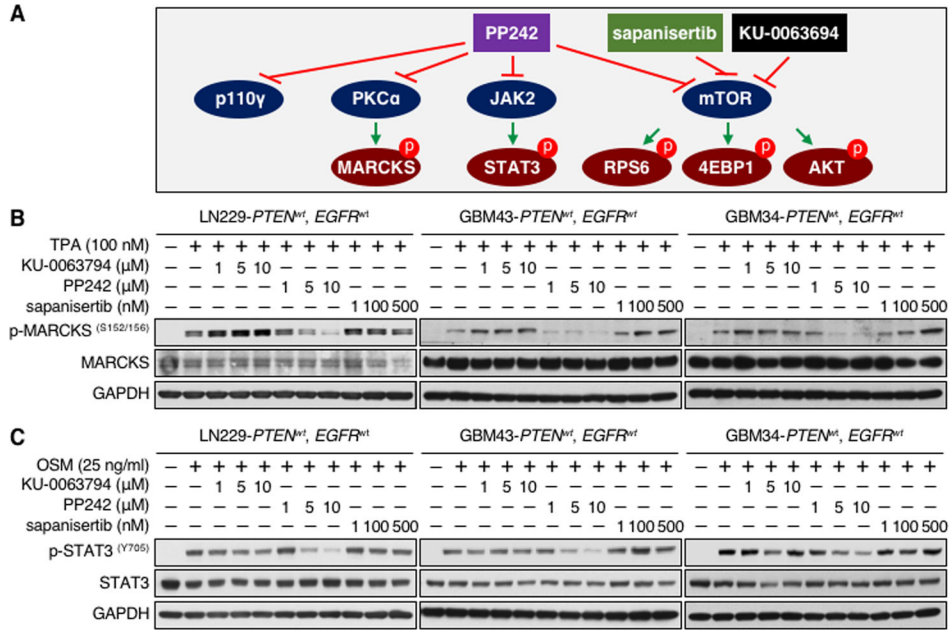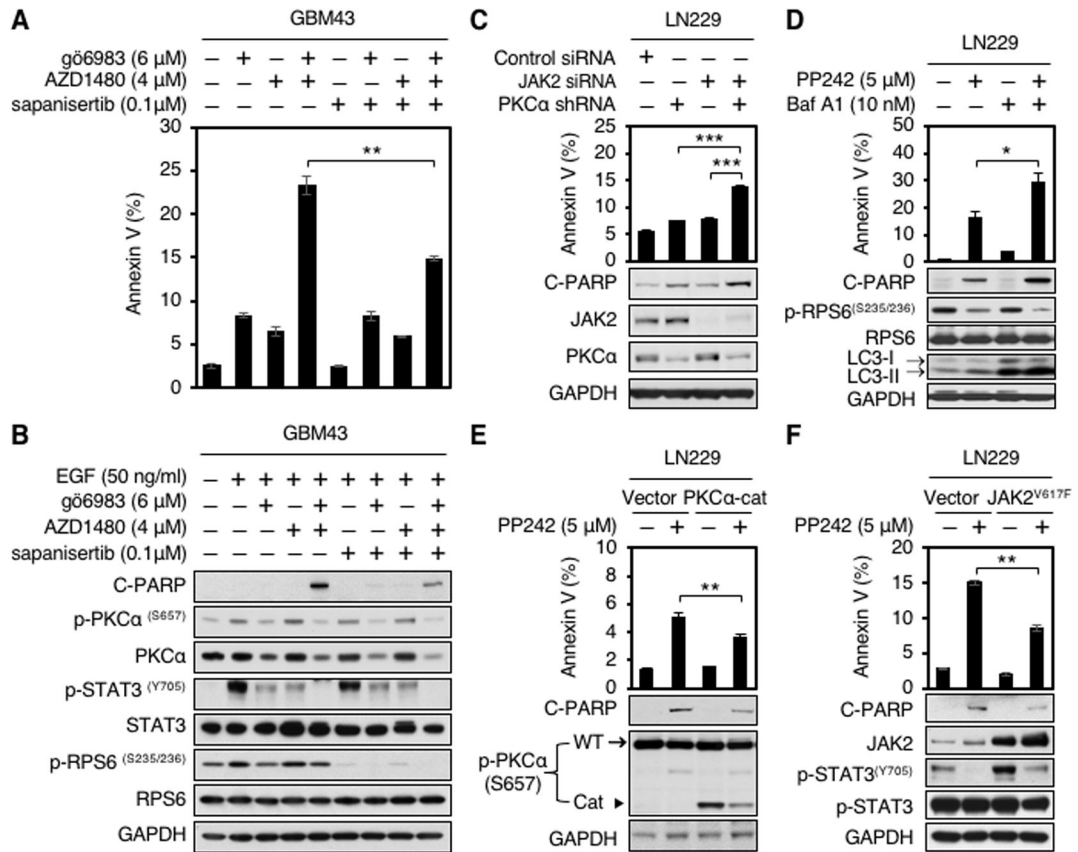
Figure 2.
PP242 inhibits mTOR, PKCα, and STAT3. **A,** Cartoon: PP242 inhibits PKCα, JAK2, and p110γ in addition to mTOR, whereas sapanisertib and KU-0063794 do not. **B and C,** LN229 parent, GBM43, and GBM34 cells were treated with KU-0063794, PP242, and sapanisertib at indicated doses for 24 hours. *PTEN and EGFR* status in glioma cell lines is shown (wt, wild type). Cells were harvested, lysed, and analyzed by western blot with indicated antibodies. TPA (100 nM) or OSM (25 ng/ml) were added 30 minutes before harvest.
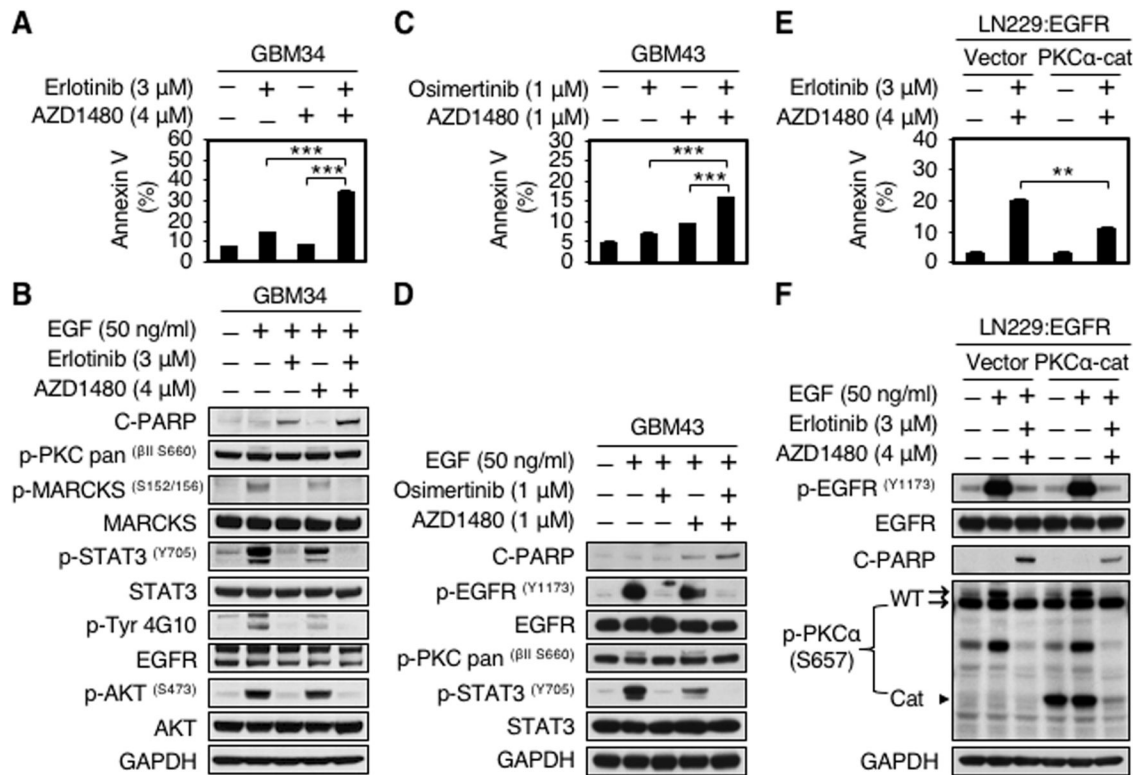
Figure 3.
Inhibition of PKC or JAK2 but not mTOR induces apoptosis in glioma cells. LN229 parent cells were treated with PKC inhibitor gö6983, JAK2 inhibitor AZD1480, or mTOR inhibitor sapanisertib at indicated doses for 72 hours. **A,** Proliferation was measured by WST-1 assay. Data shown represent mean ± SD (percentage of growth relative to DMSO-treated control) of triplicate measurements. **B,** Apoptosis was analyzed by flow cytometry for annexin V. Data shown represent mean ± SD (percentage of apoptotic cells relative to DMSO-treated control) of triplicate measurements. **C,** An aliquot of each lysate was analyzed by western blot with antibodies indicated. Blot representative of two independent experiments is shown. TPA (100 nM) was added 30 minutes before harvest.
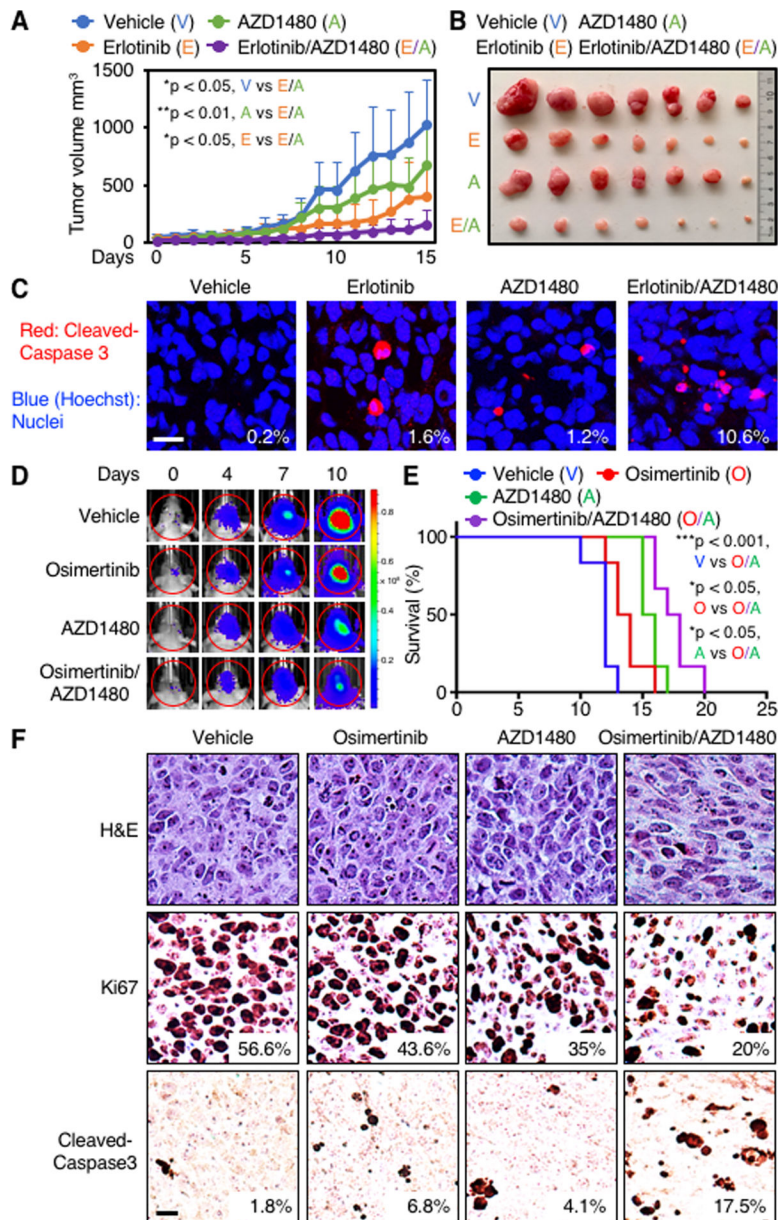
Figure 4.
Apoptosis induced by PP242 requires blockade of PKCα and JAK2. **A,** GBM43 cells were
treated with PKC inhibitor gö6983, JAK2 inhibitor AZD1480, TORKi sapanisertib, gö6983
plus AZD1480, gö6983 plus sapanisertib, AZD1480 plus sapanisertib, or gö6983 plus
AZD1480 and sapanisertib at indicated doses for 48 hours. Apoptosis was analyzed by flow
cytometry for annexin V. Data shown represent mean ± SD (percentage of apoptotic cells
relative to DMSO-treated control) of triplicate measurements (Student's *t* test, p = 0.0007,
DMSO versus gö6983 plus AZD1480; p = 0.0011, gö6983 versus gö6983 plus AZD1480; p
= 0.003, AZD1480 versus gö6983 plus AZD1480; p = 0.0007, sapanisertib versus gö6983
plus AZD1480; p = 0.0026, gö6983 plus sapanisertib versus gö6983 plus AZD1480; p =
0.0013, AZD1480 plus sapanisertib versus gö6983 plus AZD1480; p = 0.0038, gö6983 plus
AZD1480 and sapanisertib versus gö6983 plus AZD1480) (**top panel**). **B,** An aliquot of
each lysate was analyzed by western blot with antibodies indicated (**bottom panel**). EGF
(50 ng/ml) was added 15 minutes before harvest. **C,** LN229 parent cells stably expressing
shRNA against PKCα were transfected with scramble siRNA or JAK2 siRNA for 72 hours.
Apoptosis was analyzed by flow cytometry for annexin V. Data shown represent mean ± SD
(percentage of apoptotic cells relative to DMSO-treated control) of triplicate measurements
(Student's *t* test, p = 0.0002, scramble siRNA versus PKCα shRNA plus JAK2 siRNA; p =
0.0004, PKCα shRNA versus PKCα shRNA plus JAK2 siRNA; p = 0.0003, JAK2 siRNA
versus PKCα shRNA plus JAK2 siRNA) (**top panel**). An aliquot of each lysate was
analyzed by western blot with antibodies indicated (**bottom panel**). Blot representative of

two independent experiments is shown. **D,** LN229 parent cells were treated with PP242, bafilomycin A1, or PP242 plus bafilomycin A1 at indicated doses for 72 hours. Apoptosis was analyzed by flow cytometry for annexin V. Data shown represent mean ± SD (percentage of apoptotic cells relative to DMSO-treated control) of triplicate measurements (Student's *t* test, p = 0.0046, DMSO versus PP242 plus Baf A1; p = 0.0324, PP242 versus PP242 plus Baf A1; p = 0.0054, Baf A1 versus PP242 plus Baf A1) (**top panel**). An aliquot of each lysate was analyzed by western blot with antibodies indicated (**bottom panel**). **E,** LN229 parent cells were transduced with empty vector, or a dominant-active allele of PKCα (PKCα-Cat). Cells were treated with 5 μM PP242 for 72 hours. Apoptosis were analyzed by flow cytometry for annexin V. Data shown represent mean ± SD (percentage of apoptotic cells relative to DMSO-treated control) of triplicate measurements {Student's *t* test, p = 0.0016, DMSO (vector) versus PP242 (vector); p = 0.0008, DMSO (PKCα-cat) versus PP242 (Vector); p = 0.0044, PP242 (PKCα-cat) versus PP242 (vector)} (**top panel**). An aliquot of each lysate was analyzed by western blot with antibodies indicated (**bottom panel**). In p-PKCα immunoblot, the top band (**arrow**) indicates endogenous PKCα, whereas the low band (**arrowhead**) indicates a dominant-active allele of PKCα (PKCα-Cat). **F,** LN229 parent cells were transfected with empty vector, or a gain-of-function mutation of JAK2 (*JAK2^{V617F}*). Cells were treated with 5 μM PP242 for 72 hours. Apoptosis were analyzed by flow cytometry for annexin V. Data shown represent mean ± SD (percentage of apoptotic cells relative to DMSO-treated control) of triplicate measurements {Student's *t* test, p = 0.0001, DMSO (vector) versus PP242 (vector); p = 0.0001, DMSO (*JAK2^{V617F}*) versus PP242 (Vector); p = 0.0014, PP242 (*JAK2^{V617F}*) versus PP242 (vector)} (**top panel**). An aliquot of each lysate was analyzed by western blot with antibodies indicated (**bottom panel**).

Figure 5.
EGFR and JAK2 inhibitors in combination induce apoptosis in part through inhibition of PKCα. **A,** GBM34 cells were treated with erlotinib, AZD1480, or erlotinib plus AZD1480 at indicated doses for 72 hours. Apoptosis was analyzed by flow cytometry for annexin V. Data shown represent mean ± SD (percentage of apoptotic cells relative to DMSO-treated control) of triplicate measurements (Student's *t* test, p = 0.0002, DMSO versus erlotinib plus AZD1480; p = 0.0004, erlotinib versus erlotinib plus AZD1480; p = 0.0005, AZD1480 versus erlotinib plus AZD1480). **B,** An aliquot of each lysate was analyzed by western blot with antibodies indicated. EGF (50 ng/ml) was added 15 minutes before harvest. **C,** GBM43 cells were treated with osimertinib, AZD1480, or osimertinib plus AZD1480 at indicated doses for 48 hours. Apoptosis was analyzed by flow cytometry for annexin V. Data shown represent mean ± SD of triplicate measurements (Student's *t* test, p = 0.0083, DMSO versus osimertinib plus AZD1480; p = 0.0005, osimertinib versus osimertinib plus AZD1480; p = 0.0001, AZD1480 versus osimertinib plus AZD1480). **D,** An aliquot of each lysate was analyzed by western blot with antibodies indicated. EGF (50 ng/ml) was added 15 minutes before harvest. **E,** LN229:*EGFR* cells were transduced with empty vector, or a dominant-active allele of PKCα (PKCα-Cat). Cells were treated with 3 μM erlotinib and 4 μM AZD1480 for 48 hours, Apoptosis was analyzed by flow cytometry for annexin V. Data shown represent mean ± SD (percentage of apoptotic cells relative to DMSO-treated control) of triplicate measurements {Student's *t* test, p = 0.0007, DMSO (vector) versus erlotinib plus AZD1480 (vector); p = 0.0005, DMSO (PKCα-Cat) versus erlotinib plus AZD1480 (vector); p = 0.0018, erlotinib plus AZD1480 (PKCα-Cat) versus erlotinib plus AZD1480 (vector)}. **F,** An aliquot of each lysate was analyzed by western blot with antibodies indicated. EGF (50 ng/ml) was added 15 minutes before harvest.

Figure 6.

EGFR and JAK2 inhibitors in combination induce apoptosis in patient-derived flank and orthotopic xenograft models. **A,** 5×10^6 GBM34 cells were injected subcutaneously in BALB/c$^{nu/nu}$ mice. After tumor establishment, seven mice in each group were treated orally once daily with vehicle (0.5% HPMC, 0.1% Tween 80 in H$_2$O), 50 mg/kg erlotinib, 15 mg/kg AZD1480, or 50 mg/kg erlotinib plus 15 mg/kg AZD1480 for 15 days. Tumor sizes were measured every day for 15 days (Student's t test, p = 0.0177, vehicle versus erlotinib plus AZD1480; p = 0.00373, AZD1480 versus AZD1480 plus erlotinib; p = 0.0457, erlotinib versus erlotinib plus AZD1480. n = 7 mice per group). **B,** Representative tumors after 15 days. **C,** Three animals from each group in (**A and B**) were euthanized on day 15. Tumors were analyzed by immunofluorescence with antibody to cleaved caspase 3 (red). Hoechst (blue) stains nuclei. The percentage of positive cells was calculated. Data shown are

mean ± SD of five microscopic fields from three tumors in each group (Student's *t* test, p < 0.0001, vehicle versus erlotinib plus AZD1480; p < 0.0001, erlotinib versus erlotinib plus AZD1480; p < 0.0001, AZD1480 versus erlotinib plus AZD1480). Scale bar: 10 μm. **D,** 7×10^4 GBM43 cells expressing firefly luciferase were injected intracranially into BALB/c$^{nu/nu}$ mice. After tumor establishment, mice were sorted into four groups and treated daily by oral gavage, with vehicle, osimertinib (25 mg/kg), AZD1480 (30 mg/kg), or osimertinib (25mg/kg) plus AZD1480 (30mg/kg). Bioluminescence imaging of tumor-bearing mice was obtained at days shown (day 0 was start of treatment), using identical emission and excitation spectra, and exposure times for each set of measurements. Dynamic measurements of bioluminescence intensity (BLI) in treated tumors over time. Regions of interest (ROIs) from displayed images were revealed on the tumor sites and quantified as maximum photons/s/cm^2 squared/steradin. Data shown represent mean of photon flux ± SD from n = 6 mice per group. **E,** Survival curves of BALB/c$^{nu/nu}$ injected intracranially with GBM43 cells. Mice treated daily by oral gavage, with vehicle, osimertinib (25 mg/kg), AZD1480 (30 mg/kg), or osimertinib (25 mg/kg) plus AZD1480 (30 mg/kg) (p = 0.0006, vehicle versus osimertinib plus AZD1480; p = 0.024, osimertinib versus osimertinib plus AZD1480; p = 0.0198, AZD1480 versus osimertinib plus AZD1480; log-rank analysis; n = 6 mice per group). **F,** Three animals from each group treated in **D** were sacrificed at endpoint. Samples were analyzed by immunohistochemistry for cleaved caspase 3. Panels show representative images. Percentage of tumor cells that stained positively for cleaved caspase 3 and Ki67 from 5 high power microscopic fields in each group is indicated. Scale bar = 10 μm.